Membrane curvature generation by a C-terminal amphipathic helix in peripherin-2/rds, a tetraspanin required for photoreceptor sensory cilium morphogenesis

Nidhi Khattree, Linda M. Ritter and Andrew F. X. Goldberg*

Eye Research Institute, Oakland University, Rochester, MI 48309, USA

*Author for correspondence (goldberg@oakland.edu)

Accepted 5 July 2013
Journal of Cell Science 126, 4659–4670

doi: 10.1242/jcs.126888

Summary

Vertebrate vision requires photon absorption by photoreceptor outer segments (OSs), structurally elaborate membranous organelles derived from non-motile sensory cilia. The structure and function of OSs depends on a precise stacking of hundreds of membranous disks. Each disk is fully (as in rods) or partially (as in cones) bounded by a rim, at which the membrane is distorted into an energetically unfavorable high-curvature bend; however, the mechanism(s) underlying disk rim structure is (are) not established. Here, we demonstrate that the intrinsically disordered cytoplasmic C-terminus of the photoreceptor tetraspanin peripherin-2/rds (P/rds) can directly generate membrane curvature. A P/rds C-terminal domain and a peptide mimetic of an amphipathic helix contained within it each generated curvature in liposomes with a composition similar to that of OS disks and in liposomes generated from native OS lipids. Association of the C-terminal domain with liposomes required conical phospholipids, and was promoted by membrane curvature and anionic surface charge, results suggesting that the P/rds C-terminal amphipathic helix can partition into the cytosolic membrane leaflet to generate curvature by a hydrophobic insertion (wedging) mechanism. This activity was evidenced in full-length P/rds by its induction of small-diameter tubulovesicular membrane foci in cultured cells. In sum, the findings suggest that curvature generation by the P/rds C-terminus contributes to the distinctive structure of OS disk rims, and provide insight into how inherited defects in P/rds can disrupt organelle structure to cause retinal disease. They also raise the possibility that tethered amphipathic helices can function for shaping cellular membranes more generally.

Key words: Amphipathic helix, Membrane curvature, Photoreceptor, Retinal degeneration, Tetraspanin, Intrinsically disordered

Introduction

The ultrastructural architecture of vertebrate photoreceptor light-receptive organelles has intrigued biologists for more than 50 years. These highly membranous structures, commonly known as outer segments (OSs), derive from non-motile cilia of both rod and cone photoreceptors and form the basis for image-related light detection. OSs convert light into neuronal signals through a G-protein-mediated phototransduction cascade, which has been well described in recent years (Arshavsky and Burns, 2012; Palczewski, 2012). This process occurs on and adjacent to a stacked array of photopigment-filled membranous disks. Each stack includes hundreds of such disks, and is partially renewed each day by a balanced process of disk morphogenesis and shedding. Defects in OS structure and/or renewal profoundly impair photoreceptor function and viability and generate a variety of retinal diseases (Berger et al., 2010; Sung and Chuang, 2010).

The mature rod OS disk is a distinct subcellular compartment that comprises a flattened central lamellar region bounded by a rim structure along its periphery. It has been proposed that the distortion of rim membranes into energetically unfavorable high-curvature bends is stabilized by adhesive protein interaction within rim lumens – because classically prepared specimens display electron-dense internal densities, but lack protein coats (Corless and Fetter, 1987). A recent cryoelectron tomographic study confirms that distinct rim domains are present in unfixed tissue and verifies the high curvature of these structures (Nickell et al., 2007). To date, however, the mechanism by which disk rim structure is created and stabilized remains unknown.

Membrane shaping and remodeling is a crucial issue for all cells, and our understanding of how membranous organelle morphologies are generated has improved significantly in the past decade (Farsad and De Camilli, 2003; Shibata et al., 2009; McMahon et al., 2010). Membrane morphology is mainly governed by interaction with proteins (Graham and Kozlov, 2010), and the amphipathic helix (AH) has emerged as the motif most frequently associated with curvature generation (Shibata et al., 2009; Drin and Antonny, 2010). These structures can function as wedges to increase the surface area of one bilayer leaflet and/or act as anchors for bilayer-deforming scaffolding proteins. We report here that a robust membrane-remodeling activity is associated with an AH in the C-terminal domain of the retinal tetraspanin peripherin-2/rds (P/rds; also known as tetraspanin-22 and PRPH2). This self-associating integral membrane protein is localized to disk rims (Molday et al.,

1987), is essential for OS morphogenesis (Travis et al., 1992), and is responsible for a broad variety of inherited retinal diseases, including *retinitis pigmentosa* and macular dystrophies (Boon et al., 2008). Although advances have been made for understanding its structure and cellular role, the molecular function of P/rds has remained an open question (Goldberg, 2006; Farjo and Naash, 2006; Conley and Naash, 2009). The localization of P/rds at disk rim domains has fuelled speculation that it functions to stabilize this structural feature (Molday et al., 1987; Arikawa et al., 1992). Tetraspanin proteins act variously as organizers of membrane-mediated signaling networks or as structural scaffolding for specialized membrane domains (Berditchevski and Rubinstein, 2013). The current findings are most consistent with the latter function, and suggest a direct role for P/rds in generating and/or sensing the curvature associated with creation and maintenance of OS membrane architecture.

Results

We were prompted to investigate an inducible AH in the P/rds cytoplasmic C-terminus by the previous finding that transgenic expression of this domain disrupts OS membrane architecture in a highly specific fashion (Tam et al., 2004). This AH was initially identified by Battaglia and colleagues (Boesze-Battaglia et al., 1998; Boesze-Battaglia et al., 2000), and was suggested to promote membrane fusion events important for disk morphogenesis and/or shedding. Numerous precedents for AH function in shaping membranes (Drin and Antonny, 2010) led us to formulate an alternative hypothesis – that this feature contributes to the membrane curvature that defines rod OS disk structure. Fig. 1 presents an overview of the AH within the context of P/rds domain structure and the cytoplasmic C-terminus (Fig. 1A,B), and the rod OS organelle (Fig. 1D–G). The cytoplasmic orientation of the P/rds C-terminal domain (Fig. 1G) has been previously determined (Connell and Molday, 1990). Amino acid sequence alignments and helical wheel representations (Fig. 1B–C) illustrate the conservation and strongly amphipathic character present in this motif. A large hydrophobic moment (<μH>=0.618) combined with a charged hydrophilic face are predicted to drive folding of this region into a stable α-helix when bound to negatively charged membranes

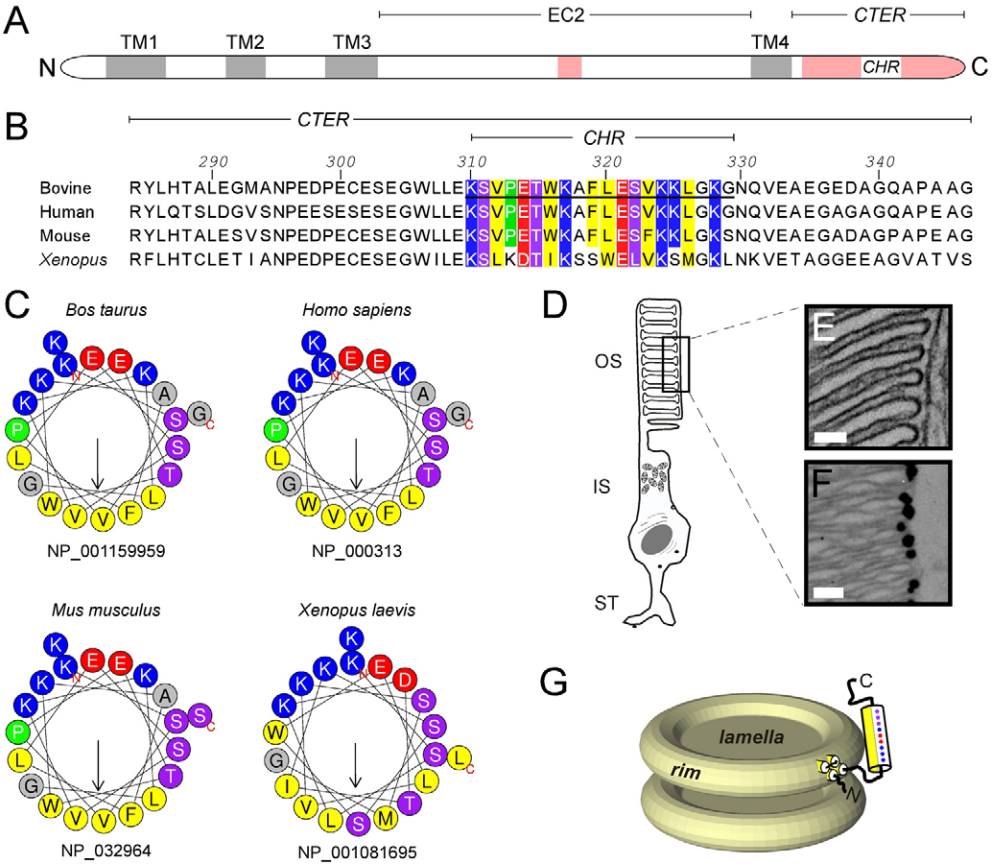

Fig. 1. A tethered amphipathic helix in P/rds is well positioned to create membrane curvature. (A) Domain structure of full-length P/rds. Transmembrane domains (TM) are shaded gray (Connell and Molday, 1990); intrinsically disordered regions are shaded pink (Ritter et al., 2005); extracellular 2 (EC2) domain mediates oligomerization (Loewen and Molday, 2000; Goldberg et al., 2001). (B) Sequence alignment of the C-termini of commonly studied P/rds orthologs. The recombinant protein (CTER) and synthetic peptide (CHR; underlined) used in this study were based on the bovine sequence. (C) Helical wheel representations were generated from the aligned C-termini of the indicated sequences (retrieved from National Center for Biotechnology Information) using the HELIQUEST server (Gautier et al., 2008). Yellow, hydrophobic residues; purple, serine and threonine; blue, basic residues; red, acidic residues; green, proline; gray, other residues. Arrows indicate relative hydrophobic moments. (D) The vertebrate rod photoreceptor OS encloses hundreds of flattened membranous disks arrayed along the axis of incoming light (IS, inner segment; ST, synaptic terminal). Disk edges are defined by rim regions which contain concentrated P/rds. (E) Plastic-embedded murine OS. Scale bar: 50 nm. (F) Postembedding immunogold labeled murine OS. Scale bar: 100 nm. (G) The AH residing within the otherwise disordered C-terminal domain is tethered in close proximity to the disk rim by the integral membrane portion of the protein.

(Drin and Antonny, 2010). This prediction is supported by experiments using a synthetic peptide in the presence of a membrane mimetic (Boesze-Battaglia et al., 1998; Boesze-Battaglia et al., 2000).

We used a standard approach for evaluating the hypothesis that the P/rds C-terminal AH can promote membrane curvature generation. Liposomes of defined size were extruded using a mixture of synthetic dioleoyl phospholipids in a molar ratio mimicking that of OS disks ('dioleoyl disk-mix' liposomes as detailed in the Materials and Methods). Vesicles were incubated with a 20 amino acid (AA) synthetic peptide corresponding to the P/rds C-terminal AH (C-terminal helical region; CHR), using a range of protein-to-lipid molar ratios (P:L) commonly applied for assaying curvature induction (Taneva et al., 2012). The vesicles were fixed, embedded in plastic resin, and visualized by transmission electron microscopy (TEM). Fig. 2A–D shows a TEM analysis of plastic-embedded liposomes that were incubated without (A) or with (B–D) increasing amounts of peptide (P:L=1:45, 1:15, 1:5, respectively). The images (and histograms) illustrate that the P/rds C-terminal AH increased membrane curvature, reducing the mean vesicle diameter by >40% as P:L molar ratio was increased. Although circular and ellipsoid vesicular profiles were most common, small-diameter tubules derived from larger liposomes were also frequently observed at intermediate P:L ratios.

Given that the isolated AH generated membrane curvature, we next asked whether it remains active within the context of its normal domain: the P/rds C-terminus. We therefore combined dioleoyl disk-mix liposomes with a purified recombinant version of the P/rds C-terminal domain (CTER) and used negative staining TEM to assay liposome remodeling. Generation and purifications of recombinant proteins used in this study are documented in supplementary data (supplementary material Fig. S1). Negative staining of liposomes deposited directly onto grids offers the advantage of direct sample processing and visualization, and is the most commonly used assay for membrane curvature generation. Fig. 3 demonstrates that CTER potently remodeled dioleoyl disk-mix liposomes in a concentration-dependent manner (Fig. 3A–C compared with 3G). The highest concentration of CTER (C; P:L=1:10) reproducibly created long tubules (mean diameter ~21.9 nm), that were frequently still attached to the liposomes from which they were derived. By comparison, CHR (the AH synthetic peptide) generated membrane curvature in a less-potent fashion (Fig. 3D–F compared with 3G). Although some differences in vesicle appearance are expected for the different assay methods,

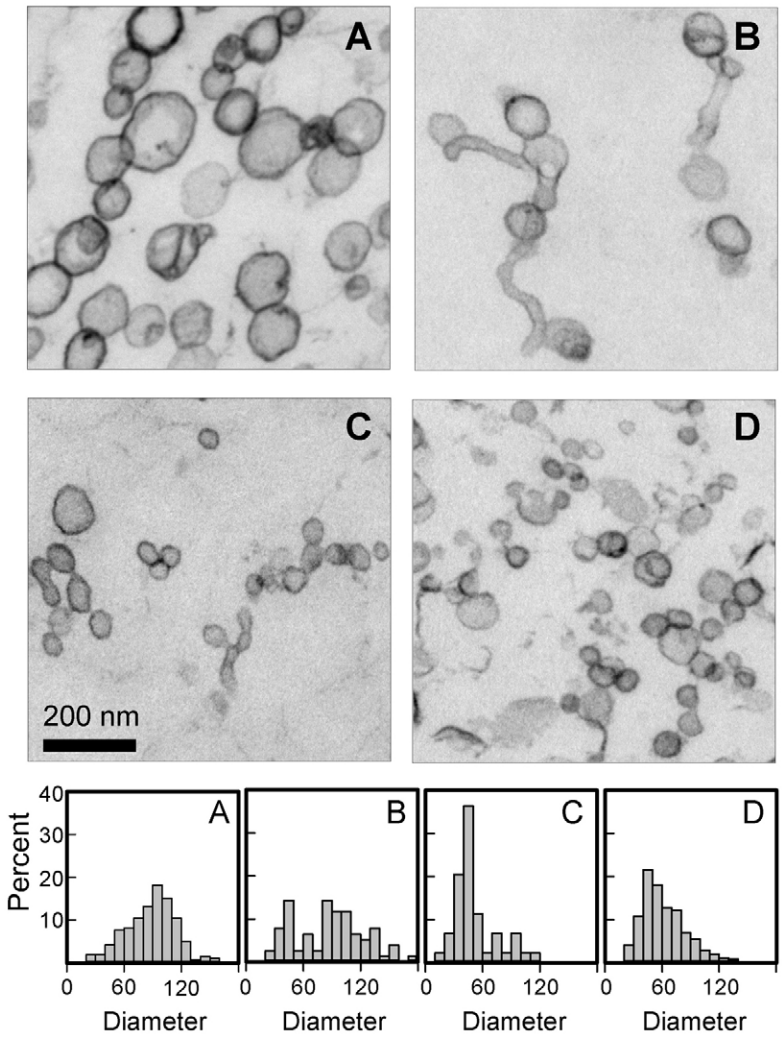

Fig. 2. A synthetic peptide corresponding to the P/rds C-terminal AH remodels liposomes. Electron microscopy of fixed, resin embedded, and sectioned dioleoyl disk-mix liposomes (DOPC:DOPE:DOPS:CHOL; 5:4:1:1). Freshly extruded liposomes (100 nm, 0.5 mM) were incubated with synthetic peptide CHR (KSVPETWKAFLESVKKLGKG), corresponding to the C-terminal AH of P/rds, at the indicated protein:lipid molar ratios (P:L): (A) no peptide; (B) 1:45; (C) 1:15; (D) 1:5 before fixation and embedding. Liposome diameters were progressively reduced with increasing amounts of peptide. Tubules were commonly observed at lower peptide concentrations.

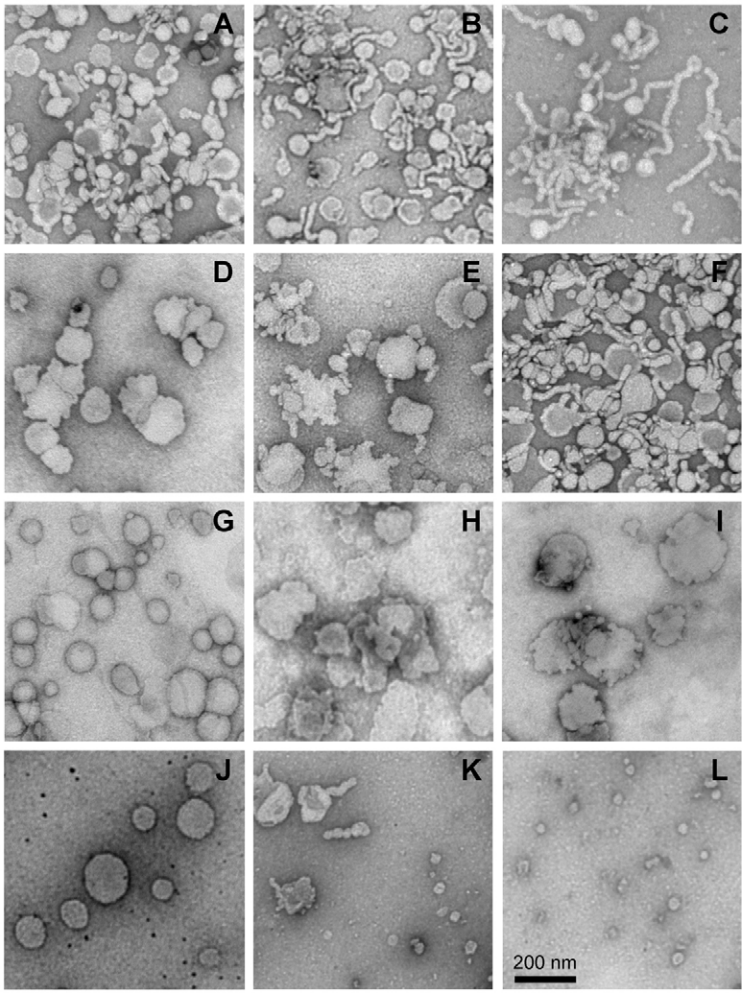

Fig. 3. Induction of membrane curvature by the P/rds C-terminal cytoplasmic domain. TEM of negatively stained liposomes (A–L). Freshly extruded disk-mix liposomes (100 nm, 0.5 mM) were incubated with purified recombinant CTER, synthetic peptide CHR or purified recombinant romCTER at the indicated P:L molar ratios. (A) 1:90 CTER; (B) 1:30 CTER; (C) 1:10 CTER; (D) 1:90 CHR; (E) 1:30 CHR; (F) 1:10 CHR; (G) no protein; (H) 1:30 romCTER; (I) 1:10 romCTER. Alternatively, liposomes extruded using a ROS lipid extract (100 nm, 0.5 mM) were incubated with purified recombinant CTER, at the indicated P:L molar ratios: (J) no protein; (K) 1:30 CTER; (L) 1:10 CTER. Blebbing, tubulation and reduced vesicle diameters were reproducibly induced in disk-mix liposomes by CTER and CHR as a function of protein and peptide concentrations. Only slight blebbing was observed at the highest concentrations of romCTER assayed. CTER and CHR also generated membrane curvature in liposomes generated using a lipid extract of purified ROS membranes. Liposomes generated from OS lipids had a similar appearance to those created from dioleoyl disk-mix lipids in the absence of added protein.

the negative staining results were in reasonably good agreement with the TEM data from aldehyde-fixed vesicle cross-sections (i.e. compare Fig. 3F, P:L=1:10, with Fig. 2C, P:L=1:15). As a negative control, we tested whether a purified recombinant version of the rom-1 C-terminal domain (romCTER) could also remodel membranes. Rom-1 (also known as tetraspanin-23) is a P/rds homolog (Bascom et al., 1992), which appears to regulate P/rds activity for OS biogenesis in a subtle and uncertain fashion. Despite its high homology, it is not required for OS biogenesis, is unable to complement P/rds loss-of-function (Clarke et al., 2000) and is not predicted to form an AH in this region (supplementary material Fig. S1). We found little or no curvature induction by romCTER at any concentration tested (Fig. 3H,I compared with 3G). To further investigate the notion that the P/rds C-terminal domain can generate membrane curvature for disk rim morphology, we tested CTER activity on liposomes generated using lipids extracted directly from purified OS membranes. CTER generated high curvature in these liposomes as well (Fig. 3K,L compared with 3J). Although tubulation was observed at lower concentrations, higher P:L ratios drove nearly complete vesiculation (mean diameter ~30.9 nm). In the absence of added protein, liposomes generated from OS lipids looked similar to those created from synthetic dioleoyl disk-mix lipids (Fig. 3J compared with 3G).

The membrane-remodeling activity observed for CTER and CHR suggested that a hydrophobic insertion mechanism was responsible for curvature generation – a wedging of the induced AH into the cytosolic leaflet of the membrane. Curvature generation by wedging is proposed to include both hydrophobic and electrostatic contributions, and can be enhanced by defects in lipid-headgroup packing (Campelo et al., 2008). We used an established flotation assay (Drin et al., 2007) to characterize CTER association with liposomes; this method avoids pitfalls associated with vesicle pelleting. Because curvature-generating proteins also typically sense membrane curvature, we addressed this possibility by measuring association of CTER with liposomes of varied curvature (diameter). Fig. 4A illustrates that the amount of CTER that bound to 30 nm, 100 nm, 200 nm and 400 nm dioleoyl disk-mix liposomes was: 77.7±17.2%, 66.3±15.3%, 55.7±8.7% and 45.6±9.3%, respectively (mean± s.d., $n \geq 4$). Thus, CTER membrane binding varied up to ~1.7-fold with vesicle size (30 nm versus 400 nm; $P=0.003$). This dependence is relatively weak compared with proteins that have an essential function as curvature sensors, which typically bind in an all-or-none manner over the size range we tested (Bigay et al., 2005). The modest curvature-sensing activity displayed by CTER is consistent with a primary function for curvature generation. If curvature was induced by wedging of the AH into a single membrane leaflet, we expected that bilayer integrity would be preserved – because full membrane thickness would not be compromised. Such was found to be the case; liposomes

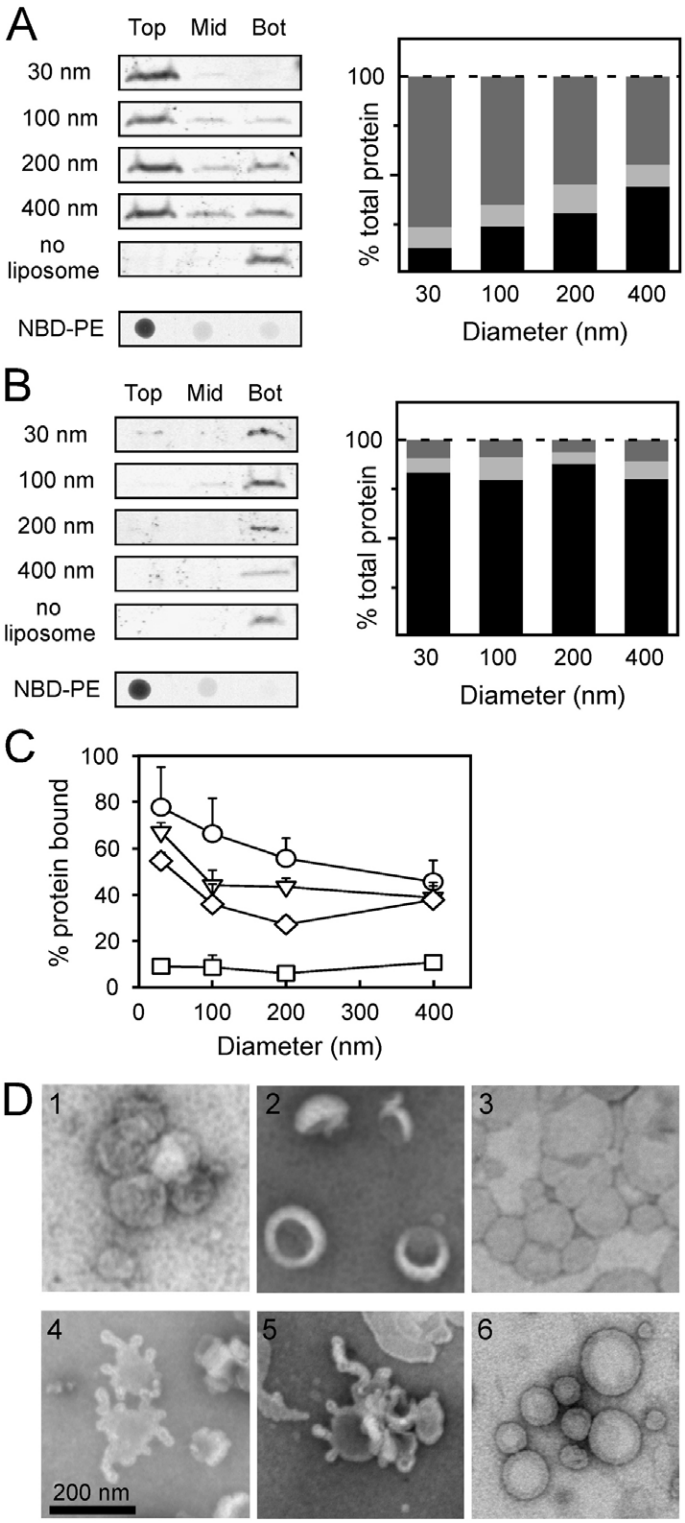

Fig. 4. CTER association with membranes requires lipid disorder and is promoted by membrane curvature and surface charge. (A) CTER (0.75 μM) was incubated with dioleoyl disk-mix liposomes (0.75 mM phospholipid) of varied size (or without liposomes), overlaid with sucrose solution and centrifuged. Top, middle (Mid) and bottom (Bot) fractions were collected and assayed by western and dot blots to quantify CTER. A representative western blot experiment is shown. Fluorescence-spot assay of NBD-PE was used to measure liposome content of each fraction. Liposomes (>95%) were always associated with 'Top' fractions; a representative NBD-PE assay for one experiment using 400 nm liposomes is shown. Graph bars represent the distribution of CTER in the top (dark gray), middle (light gray) and bottom (black) fractions. Data represent the means of at least four independent gradients and multiple batches of liposomes; error bars are omitted for clarity. Protein binding data (with confidence limits) is presented in Fig. 4C (circles). Membrane curvature promoted CTER association with dioleoyl disk-mix liposomes. (B) CTER association with membranes was dramatically reduced when a similar analysis was performed using neutral-ordered liposomes (POPC:POPE; 9:1). Data represent the means of at least four independent gradients and multiple batches of liposomes; error bars are omitted for clarity. Protein binding data (with confidence limits) are presented in Fig. 4C (squares). Loss of headgroup packing defects (lipid disorder) essentially eliminated CTER association. (C) Percentage total protein bound is plotted as a function of liposome diameter. Plots compare CTER association with: dioleoyl disk-mix (circles), neutral dioleoyl disk-mix (inverted triangles), and neutral/ordered (squares) liposomes, and E321, K324A CTER mutant binding to dioleoyl disk-mix (diamonds) liposomes. Data points represent the means (+ s.d.) of at least three independent gradients and multiple batches of liposomes. CTER association with membranes required headgroup packing defects introduced by lipid disorder and was promoted by membrane curvature and electrostatic contributions. (D) Curvature generation assessed by negative staining TEM. Neutral-ordered 100 nm liposomes (panels 1–3) or dioleoyl disk-mix 100 nm liposomes (panels 4–6) were incubated with no protein (panels 3,6), or with purified recombinant E321L,K324A mutant CTER (panels 1,4) or WT CTER (panels 2,5) at P:L molar ratios of 1:20.

remained impermeable to a small solute (calcein), even in the presence of a high concentration of CTER (supplementary material Fig. S2). We next performed a flotation analysis using liposomes generated from a neutral-ordered mix of phospholipids (composition detailed in the Materials and Methods). This mix largely lacks conically shaped lipids and completely lacks anionic lipids; it therefore generates liposomes with surfaces that do not have a net charge and are relatively free of headgroup packing defects. This is of interest because the native membranes in which P/rds resides contain an abundance of conical and anionic lipids (Anderson and Maude, 1970). We observed a dramatic reduction in CTER association with these membranes (Fig. 4B); the amount of protein that bound to the 30 nm, 100 nm, 200 nm and 400 nm liposomes was: 9.2±2.9%,

8.8±5.2%, 6.2±2.3% and 10.9±2.9%, respectively (mean ± s.d., $n \geq 4$). Thus, little protein associated with the neutral-ordered liposomes, regardless of membrane curvature. These results suggest that headgroup packing defects and electrostatic interactions are essential for association of CTER with membranes. To examine the importance of electrostatic interactions alone, we repeated the flotation analysis, this time using neutral dioleoyl disk-mix liposomes (lacking anionic lipids). Fig. 4C (inverted triangle versus circles) shows that CTER had less tendency to bind liposomes when they lacked surface charge. Statistically significant differences ($P \leq 0.05$) were evident for liposomes of intermediate diameters (100 nm, 200 nm). We also examined the contribution of electrostatic forces in an independent manner, using a mutant variant of CTER (E321L,K324A). A previous study found that neutralization of two charged residues in this variant abrogates its fusogenic activity as a GST-fusion protein *in vitro*, but preserves other properties (Ritter et al., 2004). We speculated that E321L,K324A CTER would retain the ability to associate with dioleoyl disk-mix (anionic) liposomes, although perhaps with less avidity than WT CTER. We generated purified recombinant E321L,K324A CTER (supplementary material Fig. S1) and used it to perform flotation analyses. Relative to WT CTER, the E321L,K324A mutant showed less tendency to associate with dioleoyl disk-mix liposomes (Fig. 4C; diamonds versus circles). Statistically significant differences ($P \leq 0.05$) were evident for liposomes of all diameters except the largest. These data, similar to those generated using WT CTER and neutral dioleoyl disk-mix liposomes, are consistent with a role for electrostatic interactions in promoting protein–liposome interaction. Taken together, the flotation experiments indicate that lipid disorder is a key mediator of CTER association with membranes, and that this interaction can be influenced by membrane curvature (probably through the introduction of packing defects) and by membrane surface charge (mediated by charged residues on the induced AH hydrophilic face). These properties are consistent with a hydrophilic insertion mechanism of curvature generation (McMahon and Gallop, 2005; Campelo et al., 2008). To examine whether reduced association between CTER and vesicles could impact membrane remodeling, liposomes (100 nm) incubated with WT or E321L,K324A CTER at a P:L ratio of 1:20 were assessed by negative-staining TEM. Fig. 4D demonstrates that neither protein induced membrane curvature when combined with neutral-ordered liposomes (panels 1 and 2 versus 3), but that each generated modest tubulation when combined with dioleoyl disk-mix liposomes (panels 4 and 5 versus 6). These findings suggest that protein association with liposomes was required for curvature generation, but that the modestly reduced tendency of the E321L,K324A mutant to associate with vesicles did not impair its ability to remodel membranes.

Given the *in vitro* effects of the P/rds C-terminal domain for generating membrane curvature, we were interested to know whether similar activity could be detected in cellulo. A variety of previous studies have shown that full-length P/rds expressed in cultured (COS-1) cells is properly assembled into tetrameric complexes (Goldberg et al., 1995), which can polymerize into heterogeneous higher-order species (Loewen and Molday, 2000). Here, we used AD293 cells (which lack T-antigen) to reduce the potential for protein overexpression, and applied immunocytochemical (ICC) labeling in conjunction with laser-scanning confocal microscopy (LSCM) to determine the subcellular distribution of P/rds. Results were qualitatively similar to those reported previously for COS-1 cells; P/rds was mainly associated with internal structures, often with a perinuclear density, and relatively little protein was detected at the plasma membrane. In contrast to earlier findings, however, the increased resolution provided by LSCM showed the protein to be more broadly distributed than previously observed by wide-field microscopy. Punctate labeling was distributed throughout the cytoplasm of moderately expressing cells (Fig. 5A,B); individual puncta ranged in size up to a maximum of ~0.7 μm. We performed double-labeling experiments to compare localization of P/rds with markers for the endoplasmic reticulum (ER), ER-Golgi intermediate compartment (ERGIC), Golgi complex and the endosomal recycling compartment (ERC). Fig. 5E demonstrates that contrary to previous suggestions (Goldberg et al., 1995; Ritter et al., 2004), only a small fraction of the P/rds present was colocalized with the Golgi. Moreover, P/rds reactivity did not significantly colocalize with the ER, ERGIC or ERC (Fig. 5C,D,F). The unique distribution of the heterologously expressed protein is particularly evident in 3D volume views of Z-stack images (supplementary material Movies 1–4). Altogether, this evidence indicates that P/rds is efficiently released from the secretory pathway and accumulates within distinct membranous structures. Although P/rds expressed in COS-1 cells is shown to be properly folded (Goldberg et al., 1995), we considered the possibility that this protein underwent aberrant biosynthesis in AD293, and that the puncta identified by ICC represented aggresomes, such as those formed from misfolded proteins. We tested this possibility using sedimentation analyses (Goldberg and Molday, 2000), but found that P/rds expressed in AD293 was properly folded and soluble in non-denaturing detergent (supplementary material Fig. S3), akin to that produced by overexpression of P/rds in COS-1 cells (Goldberg et al., 1995). Sedimentation analyses further demonstrated that the P/rds tetramers assembled in AD293 cells could undergo disulfide-mediated oligomerization (both in the presence and absence of rom-1), similar to that documented previously for COS-1.

Given that normally folded and assembled P/rds was packaged into discrete membranous structures in AD293, transfected cells were processed for high-resolution ultrastructural analysis by conventional TEM to investigate the morphology of the structures induced. P/rds-transfected cells showed striking foci, typically 500–1000 nm in diameter (Fig. 6A). These structures were often, but not always localized in perinuclear positions, and were never observed in mock-transfected cells or in rom-1-transfected cells (Fig. 6C,E). Multiple foci were frequently observed in a single cell (see supplementary material Fig. S4 for example), and although circular or ellipsoid boundaries were most common, irregular shapes were also sometimes observed. At higher magnifications, these foci were resolved as tubulovesicular membranes (Fig. 6B; supplementary material Fig. S4B). Close examination showed that some of these membranes were organized as interconnected tubules. Individual tubules and vesicles displayed cross-sectional outer diameters of ~35 nm, although longitudinal section diameters showed more heterogeneity, with outer diameters up to ~70 nm. We also performed post-embedding immunogold labeling of P/rds-expressing AD293 cells to examine protein distribution at the ultrastructural level (supplementary material Fig. S4D–F). Similar to the ICC/LSCM results, immunogold labeling was broadly distributed within expressing cells, although perinuclear accumulations were observed somewhat less frequently. Labeling

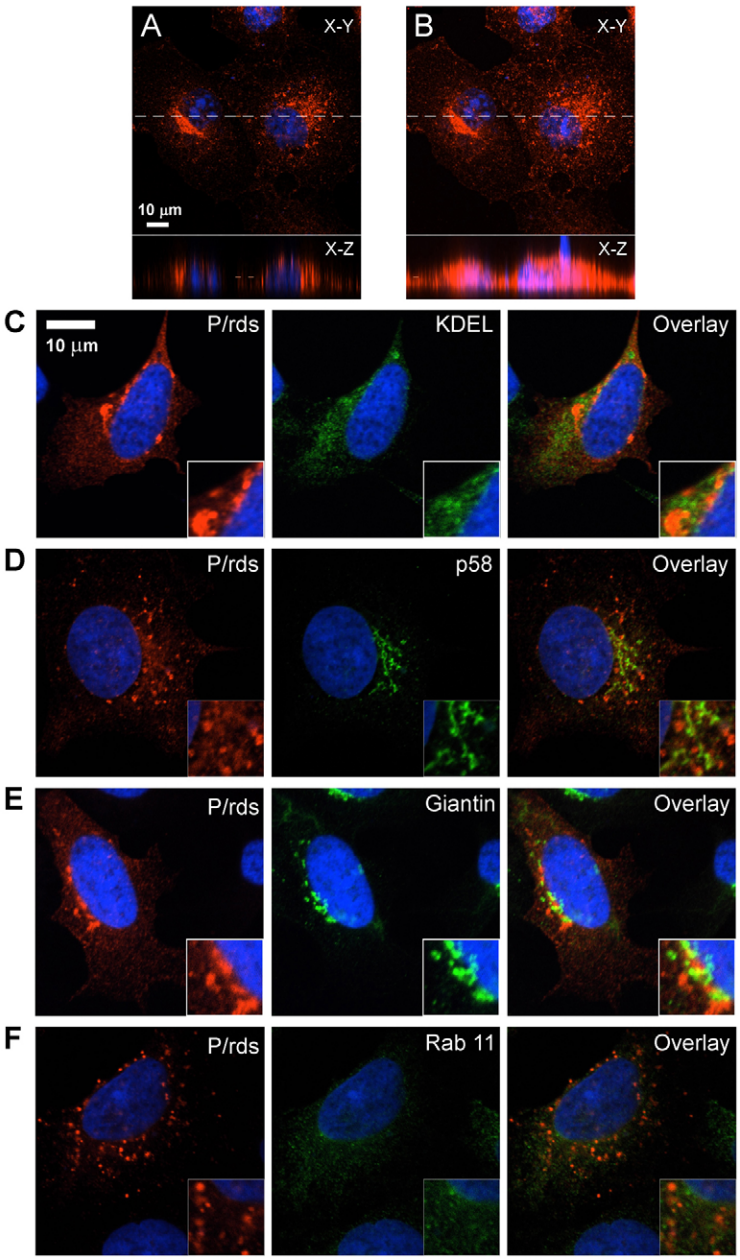

Fig. 5. P/rds expressed in cultured cells is released from the secretory pathway and accumulates in broadly distributed puncta. (A,B) LSCM analysis of AD293 cells labeled for indirect immunofluorescence with anti-P/rds MabC6 (red); nuclei are counterstained with Hoechst 33342 (blue). (A) Single optical section and (B) maximal projection from a 6.8-μm-thick *Z*-stack imaged from cells expressing a moderate level of protein are shown. *X*–*Z* views show that protein was distributed throughout the cell thickness and little was delivered to the cell surface. *X*–*Z* planes at 500% zoom. (C–F) LCSM analysis of AD293 cells double-labeled for P/rds (red) and membranous organelle markers (green), including ER (KDEL; C), ERGIC (p58; D), Golgi (giantin; E) and ERC (Rab 11; F). Nuclei are counterstained with Hoechst 33342 (blue). Single optical sections from typical cells with moderate protein expression levels are shown. Although a small fraction of P/rds reactivity colocalized with the Golgi marker, the vast majority of protein is distributed in discrete puncta distinct from secretory pathway organelles. Volume views of the full *Z*-section stacks, which illustrate this more completely, are presented as supplementary material Movies 1–4.

was largely associated with internal structures; close inspection of areas containing gold particle clusters revealed circular arrays of irregularly shaped tubulovesicular structures – features consistent with those of the foci visualized by conventional TEM (supplementary material Fig. S4E). Foci frequency, cellular distribution and dimensions correlated well with those of the P/rds-dense puncta identified by ICC/LSCM, suggesting an accumulation of P/rds protein within these structures. Altogether, the data indicate that P/rds can be released from the secretory pathway to accumulate in small-diameter tubulovesicular membranes – structures that are consistent with the curvature-generating activity displayed by the isolated C-terminal domain and AH *in vitro*.

Discussion

The mechanisms that govern photoreceptor OS morphology are of longstanding interest, but have not been identified to date. This report introduces the novel idea that an inducible AH within the P/rds cytoplasmic C-terminus can contribute to the high membrane curvature of OS disk rims. We found that both CTER (the P/rds C-terminal cytoplasmic domain, which encompasses an induced AH) and CHR (a peptide mimetic of the AH region alone) increased the curvature of liposomes generated from a mixture of synthetic phospholipids (based on that of OS disks) and liposomes generated from native lipids extracted directly from purified OS membranes. Association of CTER with membranes required conical lipids, and was promoted by anionic surface charge and the presence of membrane curvature. Expression of full-length P/rds in cultured cells induced small-diameter tubulovesicular membranes contained within focal puncta, which is consistent with the *in vitro* findings. Altogether, the new observations suggest that the P/rds C-terminus contributes to generating, maintaining and/or sensing the high curvature of OS disk rim domains.

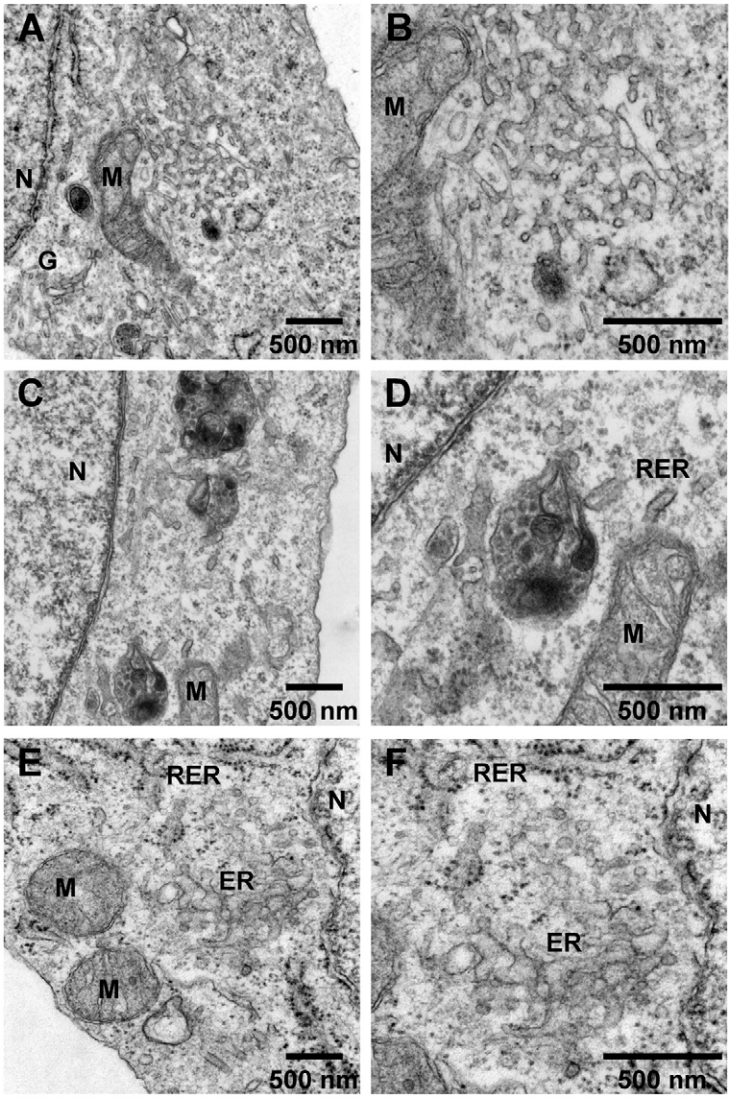

Fig. 6. Small-diameter tubulovesicular membranes induced by P/rds expression. (A) Conventional TEM imaging shows a circular cluster of membranes in a P/rds-transfected cell. Such foci were not observed in non-transfected or mock-transfected cells. (B) A higher-magnification view of the cluster shown in A reveals high curvature tubules and vesicles; cross-sectional measurements suggest an average diameter of ~35 nm. (C) Inclusions of heavily stained membranous material in a rom-1-transfected cell. Such structures were not observed in non-transfected or mock-transfected cells. Rom-1 is a P/rds homolog unable to complement P/rds functional activity (Clarke et al., 2000). (D) A higher-magnification view of one inclusion shown in C reveals irregularly packed membranes and debris. (E) Appearance of normal smooth ER membranes in a mock-transfected cell. (F) A higher-magnification view of the reticular smooth ER shown in E.

Our understanding of how membranous organelles are shaped has improved significantly in recent years. Curvature-inducing proteins play a leading role for determining membrane morphology, and the AH motif is commonly associated with regions of high curvature (Farsad and De Camilli, 2003; Shibata et al., 2009; McMahon et al., 2010). The endocytic adaptor epsin was among the first of several proteins documented to promote membrane curvature by hydrophobic insertion of an induced AH (Ford et al., 2002). This mechanism entails the coupled folding and partitioning of an AH into the cytosolic leaflet of the bilayer, with its helical axis oriented parallel to the membrane plane – creating a wedging effect that drives positive curvature (Campelo et al., 2008; Graham and Kozlov, 2010). Electrostatic interactions between basic helix residues and anionic phospholipid headgroups are proposed to overcome the energetic cost of spreading lipids apart; however, the fundamental principles governing curvature generation by AHs remain to be rigorously determined.

We evaluated the P/rds C-terminal domain (and a sub-region), using similar *in vitro* methods and observed that they each could interact with liposomes (generated either from synthetic or native lipids) to induce membrane curvature. The polymorphic shapes generated probably resulted from budding and tubulation of the original vesicles because many retained a circular profile from which tubules emanated. The most potent effects were observed when the full C-terminal domain was used in combination with liposomes generated from native lipids. The difference in behaviour between liposomes generated from native OS lipids and those from dioleoyl disk-mix lipids could reflect the unique composition of OS membranes, which includes high levels of long-chain polyunsaturated acyl chains (Miljanich et al., 1979). Phosphatidylethanolamine-containing species in particular have strongly conical shapes and create headgroup packing defects and negative curvature stress in the context of bilayer-promoting lipids (Tate and Gruner, 1987; Rajamoorthi et al., 2005; Wassall and Stillwell, 2008). The major species of conical lipids in each mixture we used (DOPE in dioleoyl disk-mix and 22:6-18:0 PE in native OS lipids) have relatively similar shapes, as indicated by their identical spontaneous intrinsic curvature values (Soubias et al., 2010). We therefore suspect that differences in the extent of disorder in their acyl chains might account for the difference in their interactions with CTER. Studies incorporating varied

amounts of 22:6-18:0 PE into liposomes might help to resolve this question. It is also possible that additional components present in the native extract (but not in the synthetic mix) have made significant contributions.

Relatively modest concentrations of P/rds CTER were required to generate *in vitro* membrane curvature, as compared with other curvature-generating proteins and with native CTER abundance in OSs. P/rds is estimated to be present in OSs at roughly 1:20 relative to the photopigment rhodopsin (Goldberg and Molday, 1996b); however, the restricted distribution of P/rds at disk rims (Molday et al., 1987) means that the protein is concentrated into a small fraction of the total disk membrane surface area. This circumstance creates a dense average packing (~4100 tetramers/μm^2) at disk rims. The present investigation found that CTER generated curvature at a P:L ratio (~1:50) within several-fold of what its native concentration is estimated to be at OS disk rims (~1:120, assuming $\sim 2\times10^6$ phospholipids/μm^2). Consistent with a hydrophobic insertion mechanism, CTER association (and curvature generation) required conical lipids and was promoted by anionic surface charge. Because curvature induction by AH-containing proteins is typically amplified by protein polymerization (Farsad and De Camilli, 2003; Campelo et al., 2008; Shibata et al., 2009), it is tempting to speculate that P/rds self-assembly might play a similar role. Although the P/rds C-terminus does not itself self-associate (Goldberg et al., 2001; Tam et al., 2004; Ritter et al., 2005), the P/rds intradiskal EC2 (extracellular 2) domain mediates several stages of functionally critical protein self-assembly (Goldberg and Molday, 1996a; Loewen and Molday, 2000; Goldberg et al., 2001; Kedzierski et al., 2001; Chakraborty et al., 2009). It is therefore possible that AH clustering and wedging (hydrophobic insertion) effects might be amplified by P/rds polymerization. Although the results presented here support a direct role for the P/rds C-terminus for disk curvature, they do not exclude the possibility that other regions of the protein (such as EC2 or transmembrane domains) could also participate in a direct fashion. Several curvature-generating proteins appear to use both wedging and scaffolding mechanisms (Shibata et al., 2009). It is therefore conceivable that EC2 domains within disk lumens might help to contour disk rim shape by a scaffolding mechanism, and future investigations will be required to examine this possibility. The development here of an in cellulo assay for P/rds contributions to curvature generation should aid such studies. The induced structures we observed were reminiscent of reticular smooth ER; however, double-labeling experiments did not find that P/rds reactivity colocalized with ER or other secretory pathway markers. We therefore propose that P/rds accumulates in membranes distinct from the main secretory pathway organelles in AD293 (and probably COS-1) cells. Although full-length P/rds translated in a cell-free system has been reported to 'flatten' microsomal vesicles (Wrigley et al., 2000), we did not observe structures that obviously resembled the flattened membranes documented previously.

Interestingly, other than the membrane-inducible AH, the ~7 kDa P/rds C-terminus is intrinsically disordered in aqueous solution (Ritter et al., 2005; Edrington et al., 2007). We have suggested previously that the plasticity present in this domain makes additional functional roles likely (Ritter et al., 2005), and several studies have found that subcellular targeting information is contained within this domain (Tam et al., 2004; Salinas et al., 2013). GFP-fusion proteins can be efficiently directed to the OS compartment by a short stretch of amino acids downstream of the inducible AH (Salinas et al., 2013). Importantly, however, the AH region is required for normal localization of GFP-fusion proteins to OS disk rims (Tam et al., 2004). The curvature sensitivity of the AH region revealed by our current study raises the possibility that localization of fusion proteins in that study was mediated by AH partitioning into the disk rim membrane, rather than by binding to rim-localized proteins. Protein localization mediated by curvature-sensing AHs is well-documented (Antonny, 2011) and our new findings suggest that additional OS proteins could be enriched at disk rims by a similar mechanism. The intrinsic disorder present in the P/rds C-terminus also raises the possibility that its AH is tethered to the membrane by a leash sufficiently long (~15 nm as a fully extended β strand) to bridge the ~7 nm gap (Nickell et al., 2007) between adjacent disk rims. In this case, AH activity might not be constrained to the disk in which the transmembrane portion of the protein is embedded, but instead (or in addition) might operate in 'trans'; studies are underway to address this issue. Such a mechanism could provide a means of stabilizing disk stack structure by directly linking adjacent disk rims; fibrils potentially serving this function have been documented, but not identified (Roof and Heuser, 1982).

Along a distinct line of investigation, Boesze-Battaglia and co-workers have hypothesized that P/rds acts as a fusogen in support of OS disk morphogenesis and/or shedding (Boesze-Battaglia et al., 1998). Their subsequent studies (Boesze-Battaglia et al., 2000; Boesze-Battaglia et al., 2003; Edrington et al., 2007) demonstrate that the P/rds C-terminus (and isolated AH) can destabilize membrane structure to promote liposome lipid and aqueous content mixing. To date, however, an integrated model for function *in situ* has not been presented and the importance of fusogenic activity for OS structure and/or renewal remains unclear. The findings reported here suggest that the previously documented fusogenic activity might reflect membrane remodeling by curvature induction, because several proteins with well-established physiological functions for curvature generation promote lipid mixing and vesicle fusion at high protein-to-lipid ratios (Drin and Antonny, 2010). The current findings also introduce the possibility that P/rds promotes membrane fission (i.e. during disk morphogenesis), because other curvature-generating AH-containing proteins are documented to perform this function *in vivo* (Boucrot et al., 2012). The present investigation found that neutralization of two conserved amino acids (E321L,K324A), previously shown to be important for CTER promotion of liposome fusion (Ritter et al., 2004), reduced membrane association, but did not have an obvious impact on curvature generation. Relative to the WT AH, the mutant has a similar net charge (+3), reduced hydrophobic moment ($<\mu H>=0.477$ versus 0.618) and increased hydrophobicity ($<H>=0.425$ versus 0.243). It is possible that the decrease in hydrophobic moment reduces free energy gain upon helix folding and partitioning into membranes, thereby weakening the interaction. At the same time, increased hydrophobicity might allow an increased depth of insertion, creating increased curvature per AH. It is also possible that the limited resolution of the curvature generation assay prevented detection of reduced activity in this mutant. Altogether, the results extend the notion that the E321L,K324A mutant is defective only in its ability to promote membrane fusion, and suggest the utility of this variant for examining the potential importance of fusogenic activity *in vivo*.

P/rds function for curvature generation offers a direct explanation for the dysmorphic OS membrane phenotypes generated by protein loss in the retinal degeneration slow (*rds*) murine model (Jansen and Sanyal, 1984; Hawkins et al., 1985). A complete loss of curvature generating activity is predicted to totally disrupt disk morphogenesis and thereby prevent OS biogenesis – a phenotype consistent with that documented for the homozygous *rds*-null mouse (Jansen and Sanyal, 1984). By contrast, a partial loss of this activity is predicted to disable disk morphogenesis in a more limited fashion – a phenotype consistent with that documented for the heterozygous *rds*-null mouse (Hawkins et al., 1985). Furthermore, loss of curvature-generating activity might be expected to affect photoreceptor subtypes differentially because disk structure in rod and cone photoreceptors appears to rely on rim formation (and P/rds) to differing extents (Steinberg et al., 1980; Arikawa et al., 1992). Indeed, P/rds haploinsufficiency impacts rods more severely than cones (Kajiwara et al., 1993; Cheng et al., 1997), which is consistent with a steeper dependence on P/rds-mediated rim curvature generation. Many pathogenic defects in P/rds represent missense mutations that result in altered proteins (Boon et al., 2008) and it is plausible that such defects could impact the C-terminus directly or indirectly (i.e. by affecting protein self-assembly). Future studies of how various disease-associated mutations affect curvature-generating activity should clarify these details.

The molecular function of P/rds has remained uncertain since its discovery 25 years ago. On the basis of the findings reported here, we propose that the C-terminus of P/rds can contribute to disk rim curvature by inserting an induced AH into the cytoplasmic leaflet of the OS disk membrane. To the best of our knowledge, P/rds is the first example of an integral membrane protein proposed to create curvature through a tethered AH. This new model can integrate a variety of previously reported protein properties including: an inducible membrane-active C-terminal AH; a high abundance; a tightly restricted distribution; an extensive self-assembly; the requirement for OS biogenesis; and a role in degenerative retinal diseases. It also raises the important questions of how P/rds curvature generation is deployed and regulated. Resolving these issues will help to improve understanding of OS structure and could provide new targets and strategies for improving visual health.

Materials and Methods

Reagents

Reagents were purchased from Fisher Scientific or Sigma-Aldrich, if not otherwise specified. Synthetic peptides were obtained from Anaspec. Lipids and cholesterol (ovine wool) were purchased from Avanti Polar Lipids, except for N-(7-nitrobenz-2-oxa-1,3-diazol-4-yl)-1,2-dihexadecanoyl-sn-glycero-3-phosphoethanolamine (NDB-PE), which was obtained from Invitrogen. AD293 cells were obtained from Stratagene.

Recombinant protein production

Expression and purification of GST–CTER, a fusion protein encoding the cytoplasmic C-terminal domain of bovine P/rds and the GST–CTER-E321L,K324A mutant variant have been described (Ritter et al., 2004). Proteolytic cleavage of GST–CTER and purification of CTER was performed as described previously (Ritter et al., 2005). The E321L,K324A variant was prepared in an identical fashion. Concentration of each protein was determined using A_{280} and a previously (experimentally) determined extinction coefficient of 14,104 $M^{-1}cm^{-1}$ (Ritter et al., 2005). A GST fusion protein was also created to produce the cytoplasmic C-terminal domain of bovine rom-1, using procedures essentially identical to those described above. A PCR fragment encoding the rom-1 C-terminal domain (amino acids 286–351) was amplified from cDNA prepared from bovine retina. The coding sequence was cloned into pGEX6P-2, and the resultant expression construct (pGEX6-ROMCTER) was used to express and purify a soluble rom-1 C-terminal domain (romCTER). Purified romCTER protein concentration was determined using A_{280} and a calculated extinction coefficient of 8480 $M^{-1}cm^{-1}$.

Liposome production and remodeling

Liposomes were generated from mixtures of synthetic phospholipids or an OS lipid extract. Dioleoyl disk-mix liposomes representative of ROS phospholipid headgroup distributions and average cholesterol content (Anderson and Maude, 1970; Fliesler and Schroepfer, 1982) contained 1,2-dioleoyl-*sn*-glycero-3-phosphocholine (DOPC), 1,2-dioleoyl-*sn*-glycero-3-phosphoethanolamine (DOPE), 1,2-dioleoyl-*sn*-glycero-3-phosphoserine (DOPS), 1-palmitoyl-2-oleoyl-*sn*-glycero-3-phosphocholine and cholesterol in a 5:4:1:1 molar ratio. Neutral-ordered liposomes contained 1-palmitoyl-2-oleoyl-*sn*-glycero-3-phosphocholine (POPC) and 1-palmitoyl-2-oleoyl-*sn*-glycero-3-phosphoethanolamine (POPE) in a 9:1 molar ratio. These lipids possess no surface charge at neutral pH and the single unsaturated acyl chain reduces headgroup packing defects (Gennis, 1989). Neutral dioleoyl disk-mix liposomes contained DOPC, DOPE and cholesterol in a 6:4:1 molar ratio. These lipids possess no surface charge at neutral pH, but retain the lipid disorder and headgroup packing defects characteristic of dioleoyl polyunsaturated phospholipids (Soubias et al., 2010; Strandberg et al., 2012). A phospholipid extract of bovine ROS was prepared by organic extraction (Folch et al., 1957), using ~10 mg of bovine ROS purified as described (Papermaster, 1982). All lipids were stored at −70℃ in chloroform under a nitrogen atmosphere. Liposomes of indicated compositions and sizes were generated by hydration of dried lipid films in buffer H (25 mM HEPES-KOH, 100 mM KCl, pH 7.4) and manual extrusion (MacDonald et al., 1991) through defined pore size polycarbonate membranes (Whatman). Size distributions were confirmed using negative-staining TEM (described below). Liposome phospholipid concentrations were determined spectrophotometrically (Bartlett, 1959). Remodeling assays were performed by incubating extruded liposomes (0.5 mM phospholipid final) with indicated ratios of synthetic peptide or recombinant protein for 1 hour at room temperature in buffer H, in a final volume of 120 µl. Synthetic peptide CHR (KSVPETWKAFLESVKKLGKG; Anaspec), was validated by mass spectrometry and judged >90% pure by high performance liquid chromatography.

Liposome morphology by transmission electron microscopy (TEM)

Liposomes to be analyzed in plastic sections were fixed for 1 hour at room temperature in 4% glutaraldehyde, 2% (w/v) osmium tetroxide in 0.1 M cacodylate buffer, pH 7.2, then were embedded in low-melt agarose and en bloc stained in 2% (w/v) uranyl acetate. Agarose blocks were embedded in Polybed 812 (Electron Microscopy Sciences) and resin sections were mounted on formvar-coated grids and poststained with 2% (w/v) uranyl acetate and lead citrate. Liposomes to be analyzed by negative staining were processed by floating glow-discharged formvar-coated grids on top of drops of liposome solution (0.5 mM in phospholipid) for 30 seconds. Grids were blotted dry, then washed twice in 2% (w/v) uranyl acetate and stained for 30 seconds in a fresh drop of the same solution. Imaging was performed using a FEI Morgagni transmission electron microscope at 80 kV, using a side-mount Hamamatsu Orca-HR digital camera driven by AMT Image Capture Engine V601 software. Size calibrations were performed using a grating replica (Electron Microscopy Sciences) to allow interpolation of all magnifications at which analyses were performed. Captured images of liposomes are presented without post-processing. Vesicle counts were performed using Image J to measure liposome diameters in randomly selected fields containing a minimum of 50 clearly defined vesicles.

Membrane binding and curvature-sensing assay

A flotation method (Matsuoka and Schekman, 2000; Drin et al., 2007) was adapted to assay CTER binding to liposomes of varied diameter. Liposomes of indicated compositions (including 0.2% NBD-PE marker and prepared as described above) were extruded through membranes with pore sizes of 400, 200, 100 and 30 nm sequentially. Vesicle diameter references are nominal and indexed to membrane pore sizes. Liposomes (0.75 mM phospholipid; 150 µl) were incubated with purified proteins (0.75 µM) in buffer H. After 10 minutes at room temperature, the samples were adjusted to 0.88 M sucrose, then were overlaid with 200 µl of 0.75 M sucrose and 50 µl of buffer H. The gradients were centrifuged for 1 hour at 55,000 rpm in a TLS-55 swinging-bucket rotor, and top (100 µl), middle (150 µl) and bottom (250 µl) fractions were collected with a Hamilton syringe. Fractions were spotted onto glass slides to assay liposome concentration (by NBD-PE fluorescence), using standard curves in conjunction with a Storm 860 Molecular Imager (Molecular Dynamics). Fractions were simultaneously subjected to western blot and/or dot-blot analysis with MabC6 and an anti-mouse infrared-dye-coupled secondary antibody to assay protein using an Odyssey Infrared Imaging system (Li-Cor). Statistical analyses were performed with SPSS (version 11.5) using a univariate analysis of variance followed by a Tukey HSD post-hoc test and a 0.05 threshold for significance.

Calcein leak assay

Relief of calcein self-quenching (Allen and Cleland, 1980) was used to determine whether CTER disrupted membranes in a non-specific fashion. Liposomes (dioleoyl disk-mix, 100 nm) were extruded at 5 mg/ml in the presence of 60 mM calcein (Sigma), 10 mM HEPES-KOH, 20 mM NaCl, pH 7.5. Untrapped calcein was removed by passing the vesicles over a Sephadex G-50 column

equilibrated with 10 mM HEPES-KOH, 100 mM NaCl, pH 7.5. Eluted vesicle fractions were identified by measuring calcein fluorescence after releasing vesicle contents by addition of 0.1% Triton X-100. CTER induction of calcein efflux from liposomes was measured by monitoring fractional fluorescence released at 520 nm, using a Shimadzu RF5000U spectrofluorimeter (excitation was at 490 nm, slit widths were 5 mm). CTER (2 μM) was combined with calcein-loaded liposomes (20 μM) at a P:L ratio of 1:10 in 10 mM HEPES-KOH, 100 mM NaCl, 1 mM EDTA, pH 7.5, and the solution was incubated at room temperature with constant stirring. Fluorescence was monitored for 90 minutes, at which time an addition of 0.1% Triton X-100 was made to determine total releasable fluorescence.

Immunocytofluorescence and laser-scanning confocal microscopy (LSCM)

AD293 cells (Stratagene) were transfected in two-well chamber slides (Lab-Tek) and processed for immunocytofluorescence analysis essentially as described (Ritter et al., 2011) using anti-P/rds MabC6 (Goldberg et al., 2001) or PabBPCT (Goldberg et al., 2007) in combination with anti-KDEL antibody (Abcam), anti-p58 antibody (kind gift from Dr Jaakko Saraste, Department of Biomedicine and Molecular Imaging Center, University of Bergen, Norway), anti-giantin antibody (Abcam), or anti-Rab11 antibody (BD Biosciences). Subsaturated image Z-stacks were acquired with a Nikon C1 Laser Scanning Confocal Microscope using a 60× oil objective (1.4 N.A.), 30 μm confocal aperture, 70 nm pixel and 0.2 μm step sizes. No adjustments (other than cropping and annotation) were made to the images. Images presented are single optical sections taken from the midpoint of a given Z-stack, unless otherwise noted. Full Z-stack volume views are provided as supplementary material.

Sedimentation assay

Velocity sedimentation of P/rds extracted from AD293 cell membranes were measured as previously described (Ritter et al., 2004) with the following modifications. AD293 cells were transfected with pcPERS and/or pcROMS (Goldberg et al., 2001), and membranes were prepared at 48 hours post-transfection essentially as described for COS-1 cells (Ritter et al., 2011). Triton X-100 membrane extracts (~100 μl from ~5×10^6 cells) were layered onto 2 ml, 5–20% sucrose gradients and centrifuged in a TLS-55 rotor (Beckman) for 16 hours at 4°C. Soluble fractions were collected by tube puncture and particulate fractions were collected by solubilization of pellets with Laemmli sample buffer. Western blotting was performed with anti-P/rds MabC6 and anti-rom-1 PabMUTT, using infrared dye-coupled secondary antibodies and an Odyssey Infrared Imaging system (Li-Cor). Pixel summation was used to generate sedimentation profiles.

Cultured cell ultrastructure and immunogold protein localization

AD293 cells in 100 mm dishes were transfected essentially as described (Ritter et al., 2004). Cells were processed for post-embedding immunogold labeling by fixation for 2 hours at room temperature in 3% PFA, 2% glutaraldehyde in 0.1M Sorensen's buffer, pH 7.4, and embedding in LR White at 55°C (Electron Microscopy Sciences). Thin sections mounted on formvar-coated grids were processed with MabC6 for immunogold labeling essentially as described previously for tissue sections (Ritter et al., 2011). TEM was performed as described above; brightness and/or contrast of some images were adjusted to facilitate comparisons.

Acknowledgements

We appreciate the expert technical assistance of Ms Loan Dang and Ms Dorothy Soronsen for electron microscopy; and Dr Svetla Taneva and Dr Guillaume Drin for liposome assay development. The anti-p58/ERGIC antibody was a generous gift of Dr Jaakko Saraste. We are grateful for helpful discussion and comments on the manuscript by Dr Miriam Goodman, Dr Guillaume Drin and Dr Bruno Antonny.

Author contributions

A.F.X.G. conceived and designed the study; N.K., L.M.R. and A.F.X.G. designed and performed experiments, analyzed and interpreted data, and prepared the manuscript.

Funding

This work was funded by the National Institutes of Health [grant numbers R01EY013246 and RR017890 to A.F.X.G.]. Deposited in PMC for release after 12 months.

Supplementary material available online at
http://jcs.biologists.org/lookup/suppl/doi:10.1242/jcs.126888/-/DC1

References

Allen, T. M. and Cleland, L. G. (1980). Serum-induced leakage of liposome contents. *Biochim. Biophys. Acta* **597**, 418-426.

Anderson, R. E. and Maude, M. B. (1970). Phospholipids of bovine outer segments. *Biochemistry* **9**, 3624-3628.

Antonny, B. (2011). Mechanisms of membrane curvature sensing. *Annu. Rev. Biochem.* **80**, 101-123.

Arikawa, K., Molday, L. L., Molday, R. S. and Williams, D. S. (1992). Localization of peripherin/rds in the disk membranes of cone and rod photoreceptors: relationship to disk membrane morphogenesis and retinal degeneration. *J. Cell Biol.* **116**, 659-667.

Arshavsky, V. Y. and Burns, M. E. (2012). Photoreceptor signaling: supporting vision across a wide range of light intensities. *J. Biol. Chem.* **287**, 1620-1626.

Bartlett, G. R. (1959). Phosphorus assay in column chromatography. *J. Biol. Chem.* **234**, 466-468.

Bascom, R. A., Manara, S., Collins, L., Molday, R. S., Kalnins, V. I. and McInnes, R. R. (1992). Cloning of the cDNA for a novel photoreceptor membrane protein (rom-1) identifies a disk rim protein family implicated in human retinopathies. *Neuron* **8**, 1171-1184.

Berditchevski, F. and Rubinstein, E. (2013). *Tetraspanins*. New York, NY: Springer Science.

Berger, W., Kloeckener-Gruissem, B. and Neidhardt, J. (2010). The molecular basis of human retinal and vitreoretinal diseases. *Prog. Retin. Eye Res.* **29**, 335-375.

Bigay, J., Casella, J. F., Drin, G., Mesmin, B. and Antonny, B. (2005). ArfGAP1 responds to membrane curvature through the folding of a lipid packing sensor motif. *EMBO J.* **24**, 2244-2253.

Boesze-Battaglia, K., Lamba, O. P., Napoli, A. A., Jr, Sinha, S. and Guo, Y. (1998). Fusion between retinal rod outer segment membranes and model membranes: a role for photoreceptor peripherin/rds. *Biochemistry* **37**, 9477-9487.

Boesze-Battaglia, K., Stefano, F. P., Fenner, M. and Napoli, A. A., Jr (2000). A peptide analogue to a fusion domain within photoreceptor peripherin/rds promotes membrane adhesion and depolarization. *Biochim. Biophys. Acta* **1463**, 343-354.

Boesze-Battaglia, K., Goldberg, A. F., Dispoto, J., Katragadda, M., Cesarone, G. and Albert, A. D. (2003). A soluble peripherin/Rds C-terminal polypeptide promotes membrane fusion and changes conformation upon membrane association. *Exp. Eye Res.* **77**, 505-514.

Boon, C. J., den Hollander, A. I., Hoyng, C. B., Cremers, F. P., Klevering, B. J. and Keunen, J. E. (2008). The spectrum of retinal dystrophies caused by mutations in the peripherin/RDS gene. *Prog. Retin. Eye Res.* **27**, 213-235.

Boucrot, E., Pick, A., Çamdere, G., Liska, N., Evergren, E., McMahon, H. T. and Kozlov, M. M. (2012). Membrane fission is promoted by insertion of amphipathic helices and is restricted by crescent BAR domains. *Cell* **149**, 124-136.

Campelo, F., McMahon, H. T. and Kozlov, M. M. (2008). The hydrophobic insertion mechanism of membrane curvature generation by proteins. *Biophys. J.* **95**, 2325-2339.

Chakraborty, D., Ding, X. Q., Conley, S. M., Fliesler, S. J. and Naash, M. I. (2009). Differential requirements for retinal degeneration slow intermolecular disulfide-linked oligomerization in rods versus cones. *Hum. Mol. Genet.* **18**, 797-808.

Cheng, T., Peachey, N. S., Li, S., Goto, Y., Cao, Y. and Naash, M. I. (1997). The effect of peripherin/rds haploinsufficiency on rod and cone photoreceptors. *J. Neurosci.* **17**, 8118-8128.

Clarke, G., Goldberg, A. F., Vidgen, D., Collins, L., Ploder, L., Schwarz, L., Molday, L. L., Rossant, J., Szél, A., Molday, R. S. et al. (2000). Rom-1 is required for rod photoreceptor viability and the regulation of disk morphogenesis. *Nat. Genet.* **25**, 67-73.

Conley, S. M. and Naash, M. I. (2009). Focus on molecules: RDS. *Exp. Eye Res.* **89**, 278-279.

Connell, G. J. and Molday, R. S. (1990). Molecular cloning, primary structure, and orientation of the vertebrate photoreceptor cell protein peripherin in the rod outer segment disk membrane. *Biochemistry* **29**, 4691-4698.

Corless, J. M. and Fetter, R. D. (1987). Structural features of the terminal loop region of frog retinal rod outer segment disk membranes: III. Implications of the terminal loop complex for disk morphogenesis, membrane fusion, and cell surface interactions. *J. Comp. Neurol.* **257**, 24-38.

Drin, G. and Antonny, B. (2010). Amphipathic helices and membrane curvature. *FEBS Lett.* **584**, 1840-1847.

Drin, G., Casella, J. F., Gautier, R., Boehmer, T., Schwartz, T. U. and Antonny, B. (2007). A general amphipathic α-helical motif for sensing membrane curvature. *Nat. Struct. Mol. Biol.* **14**, 138-146.

Edrington, T. C., 5th, Lapointe, R., Yeagle, P. L., Gretzula, C. L. and Boesze-Battaglia, K. (2007). Peripherin-2: an intracellular analogy to viral fusion proteins. *Biochemistry* **46**, 3605-3613.

Farjo, R. and Naash, M. I. (2006). The role of Rds in outer segment morphogenesis and human retinal disease. *Ophthalmic Genet.* **27**, 117-122.

Farsad, K. and De Camilli, P. (2003). Mechanisms of membrane deformation. *Curr. Opin. Cell Biol.* **15**, 372-381.

Fliesler, S. J. and Schroepfer, G. J., Jr (1982). Sterol composition of bovine retinal rod outer segment membranes and whole retinas. *Biochim. Biophys. Acta* **711**, 138-148.

Folch, J., Lees, M. and Sloane Stanley, G. H. (1957). A simple method for the isolation and purification of total lipides from animal tissues. *J. Biol. Chem.* **226**, 497-509.

Ford, M. G., Mills, I. G., Peter, B. J., Vallis, Y., Praefcke, G. J., Evans, P. R. and McMahon, H. T. (2002). Curvature of clathrin-coated pits driven by epsin. *Nature* **419**, 361-366.

Gautier, R., Douguet, D., Antonny, B. and Drin, G. (2008). HELIQUEST: a web server to screen sequences with specific α-helical properties. *Bioinformatics* **24**, 2101-2102.

Gennis, R. B. (1989). The structures and properties of membrane lipids. In *Biomembranes: Molecular Structure and Function*, pp. 36-84. New York, NY: Springer-Verlag.

Goldberg, A. F. (2006). Role of peripherin/rds in vertebrate photoreceptor architecture and inherited retinal degenerations. *Int. Rev. Cytol.* **253**, 131-175.

Goldberg, A. F. and Molday, R. S. (1996a). Defective subunit assembly underlies a digenic form of retinitis pigmentosa linked to mutations in peripherin/rds and rom-1. *Proc. Natl. Acad. Sci. USA* **93**, 13726-13730.

Goldberg, A. F. and Molday, R. S. (1996b). Subunit composition of the peripherin/rds-rom-1 disk rim complex from rod photoreceptors: hydrodynamic evidence for a tetrameric quaternary structure. *Biochemistry* **35**, 6144-6149.

Goldberg, A. F. and Molday, R. S. (2000). Expression and characterization of peripherin/rds-rom-1 complexes and mutants implicated in retinal degenerative diseases. *Methods Enzymol.* **316**, 671-687.

Goldberg, A. F., Moritz, O. L. and Molday, R. S. (1995). Heterologous expression of photoreceptor peripherin/rds and Rom-1 in COS-1 cells: assembly, interactions, and localization of multisubunit complexes. *Biochemistry* **34**, 14213-14219.

Goldberg, A. F., Fales, L. M., Hurley, J. B. and Khattree, N. (2001). Folding and subunit assembly of photoreceptor peripherin/rds is mediated by determinants within the extracellular/intradiskal EC2 domain: implications for heterogeneous molecular pathologies. *J. Biol. Chem.* **276**, 42700-42706.

Goldberg, A. F., Ritter, L. M., Khattree, N., Peachey, N. S., Fariss, R. N., Dang, L., Yu, M. and Bottrell, A. R. (2007). An intramembrane glutamic acid governs peripherin/rds function for photoreceptor disk morphogenesis. *Invest. Ophthalmol. Vis. Sci.* **48**, 2975-2986.

Graham, T. R. and Kozlov, M. M. (2010). Interplay of proteins and lipids in generating membrane curvature. *Curr. Opin. Cell Biol.* **22**, 430-436.

Hawkins, R. K., Jansen, H. G. and Sanyal, S. (1985). Development and degeneration of retina in rds mutant mice: photoreceptor abnormalities in the heterozygotes. *Exp. Eye Res.* **41**, 701-720.

Jansen, H. G. and Sanyal, S. (1984). Development and degeneration of retina in rds mutant mice: electron microscopy. *J. Comp. Neurol.* **224**, 71-84.

Kajiwara, K., Sandberg, M. A., Berson, E. L. and Dryja, T. P. (1993). A null mutation in the human peripherin/RDS gene in a family with autosomal dominant retinitis punctata albescens. *Nat. Genet.* **3**, 208-212.

Kedzierski, W., Nusinowitz, S., Birch, D., Clarke, G., McInnes, R. R., Bok, D. and Travis, G. H. (2001). Deficiency of rds/peripherin causes photoreceptor death in mouse models of digenic and dominant retinitis pigmentosa. *Proc. Natl. Acad. Sci. USA* **98**, 7718-7723.

Loewen, C. J. and Molday, R. S. (2000). Disulfide-mediated oligomerization of Peripherin/Rds and Rom-1 in photoreceptor disk membranes. Implications for photoreceptor outer segment morphogenesis and degeneration. *J. Biol. Chem.* **275**, 5370-5378.

MacDonald, R. C., MacDonald, R. I., Menco, B. P., Takeshita, K., Subbarao, N. K. and Hu, L. R. (1991). Small-volume extrusion apparatus for preparation of large, unilamellar vesicles. *Biochim. Biophys. Acta* **1061**, 297-303.

Matsuoka, K. and Schekman, R. (2000). The use of liposomes to study COPII- and COPI-coated vesicle formation and membrane protein sorting. *Methods* **20**, 417-428.

McMahon, H. T. and Gallop, J. L. (2005). Membrane curvature and mechanisms of dynamic cell membrane remodelling. *Nature* **438**, 590-596.

McMahon, H. T., Kozlov, M. M. and Martens, S. (2010). Membrane curvature in synaptic vesicle fusion and beyond. *Cell* **140**, 601-605.

Miljanich, G. P., Sklar, L. A., White, D. L. and Dratz, E. A. (1979). Disaturated and dipolyunsaturated phospholipids in the bovine retinal rod outer segment disk membrane. *Biochim. Biophys. Acta* **552**, 294-306.

Molday, R. S., Hicks, D. and Molday, L. (1987). Peripherin. A rim-specific membrane protein of rod outer segment discs. *Invest. Ophthalmol. Vis. Sci.* **28**, 50-61.

Nickell, S., Park, P. S., Baumeister, W. and Palczewski, K. (2007). Three-dimensional architecture of murine rod outer segments determined by cryoelectron tomography. *J. Cell Biol.* **177**, 917-925.

Palczewski, K. (2012). Chemistry and biology of vision. *J. Biol. Chem.* **287**, 1612-1619.

Papermaster, D. S. (1982). Preparation of retinal rod outer segments. *Methods Enzymol.* **81**, 48-52.

Rajamoorthi, K., Petrache, H. I., McIntosh, T. J. and Brown, M. F. (2005). Packing and viscoelasticity of polyunsaturated omega-3 and omega-6 lipid bilayers as seen by (2)H NMR and X-ray diffraction. *J. Am. Chem. Soc.* **127**, 1576-1588.

Ritter, L. M., Boesze-Battaglia, K., Tam, B. M., Moritz, O. L., Khattree, N., Chen, S. C. and Goldberg, A. F. (2004). Uncoupling of photoreceptor peripherin/rds fusogenic activity from biosynthesis, subunit assembly, and targeting: a potential mechanism for pathogenic effects. *J. Biol. Chem.* **279**, 39958-39967.

Ritter, L. M., Arakawa, T. and Goldberg, A. F. (2005). Predicted and measured disorder in peripherin/rds, a retinal tetraspanin. *Protein Pept. Lett.* **12**, 677-686.

Ritter, L. M., Khattree, N., Tam, B., Moritz, O. L., Schmitz, F. and Goldberg, A. F. (2011). In situ visualization of protein interactions in sensory neurons: glutamic acid-rich proteins (GARPs) play differential roles for photoreceptor outer segment scaffolding. *J. Neurosci.* **31**, 11231-11243.

Roof, D. J. and Heuser, J. E. (1982). Surfaces of rod photoreceptor disk membranes: integral membrane components. *J. Cell Biol.* **95**, 487-500.

Salinas, R. Y., Baker, S. A., Gospe, S. M., 3rd and Arshavsky, V. Y. (2013). A single valine residue plays an essential role in peripherin/rds targeting to photoreceptor outer segments. *PLoS ONE* **8**, e54292.

Shibata, Y., Hu, J., Kozlov, M. M. and Rapoport, T. A. (2009). Mechanisms shaping the membranes of cellular organelles. *Annu. Rev. Cell Dev. Biol.* **25**, 329-354.

Soubias, O., Teague, W. E., Jr, Hines, K. G., Mitchell, D. C. and Gawrisch, K. (2010). Contribution of membrane elastic energy to rhodopsin function. *Biophys. J.* **99**, 817-824.

Steinberg, R. H., Fisher, S. K. and Anderson, D. H. (1980). Disc morphogenesis in vertebrate photoreceptors. *J. Comp. Neurol.* **190**, 501-518.

Strandberg, E., Tiltak, D., Ehni, S., Wadhwani, P. and Ulrich, A. S. (2012). Lipid shape is a key factor for membrane interactions of amphipathic helical peptides. *Biochim. Biophys. Acta* **1818**, 1764-1776.

Sung, C. H. and Chuang, J. Z. (2010). The cell biology of vision. *J. Cell Biol.* **190**, 953-963.

Tam, B. M., Moritz, O. L. and Papermaster, D. S. (2004). The C terminus of peripherin/rds participates in rod outer segment targeting and alignment of disk incisures. *Mol. Biol. Cell* **15**, 2027-2037.

Taneva, S. G., Lee, J. M. and Cornell, R. B. (2012). The amphipathic helix of an enzyme that regulates phosphatidylcholine synthesis remodels membranes into highly curved nanotubules. *Biochim. Biophys. Acta* **1818**, 1173-1186.

Tate, M. W. and Gruner, S. M. (1987). Lipid polymorphism of mixtures of dioleoylphosphatidylethanolamine and saturated and monounsaturated phosphatidylcholines of various chain lengths. *Biochemistry* **26**, 231-236.

Travis, G. H., Groshan, K. R., Lloyd, M. and Bok, D. (1992). Complete rescue of photoreceptor dysplasia and degeneration in transgenic retinal degeneration slow (rds) mice. *Neuron* **9**, 113-119.

Wassall, S. R. and Stillwell, W. (2008). Docosahexaenoic acid domains: the ultimate non-raft membrane domain. *Chem. Phys. Lipids* **153**, 57-63.

Wrigley, J. D., Ahmed, T., Nevett, C. L. and Findlay, J. B. (2000). Peripherin/rds influences membrane vesicle morphology. Implications for retinopathies. *J. Biol. Chem.* **275**, 13191-13194.